UCRL-92523
PREPRINT

SMOKE INPUTS TO CLIMATE MODELS: OPTICAL PROPERTIES AND HEIGHT DISTRIBUTION FOR NUCLEAR WINTER STUDIES

Joyce E. Penner and Leonard C. Haselman, Jr.

This paper was prepared for publication in the Proceedings of the International Seminar on Nuclear War 4th Session: The Nuclear Winter and the New Defense Systems: Problems and Perspectives Erice, Italy, August 19-24, 1984. Sponsored by the Ettore Majorana Centre for Scientific Culture

April 1985

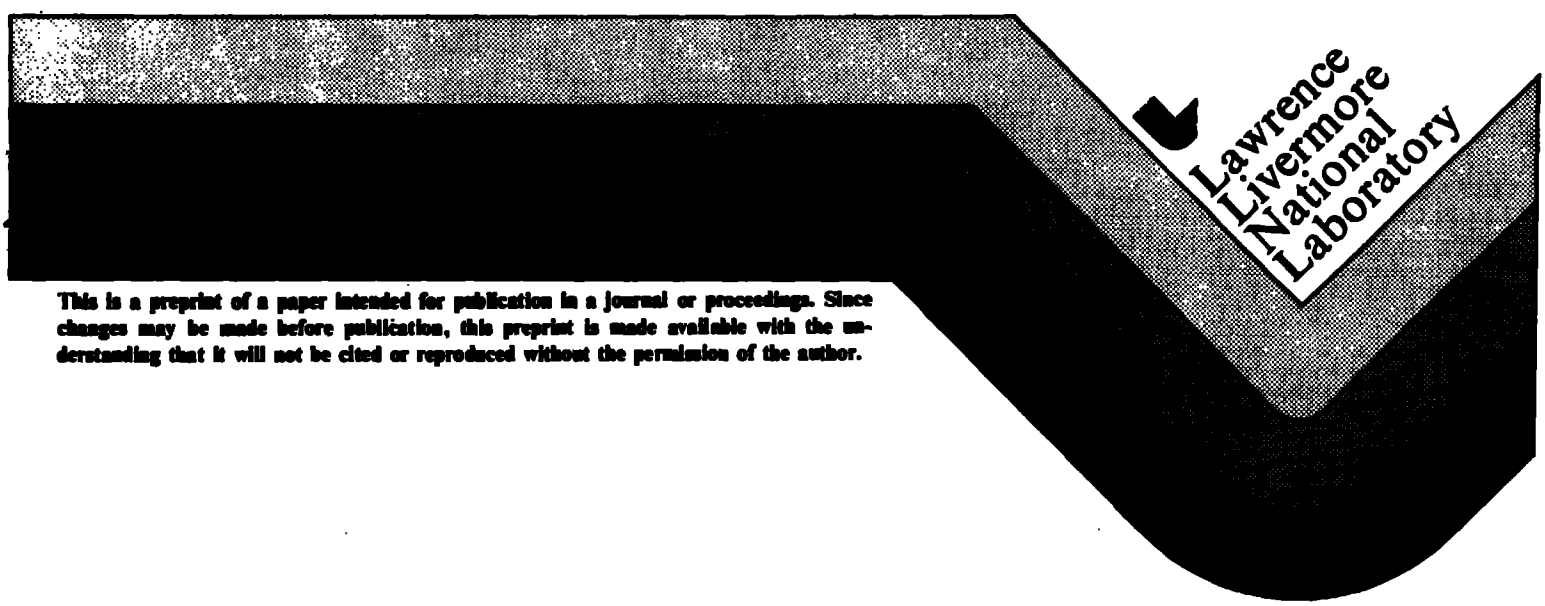

SMOKE INPUTS TO CLIMATE MODELS: OPTICAL PROPERTIES AND HEIGHT DISTRIBUTION FOR NUCLEAR WINTER STUDIES

Joyce E. Penner and Leonard C. Haselman, Jr.

Lawrence Livermore National Laboratory, University of California
Livermore, CA 94550 USA

Abstract

Smoke from fires produced in the aftermath of a major nuclear exchange has been predicted to cause large decreases in land surface temperatures. However, the extent of the decrease and even the sign of the temperature change depend on the optical characteristics of the smoke and how it is distributed with altitude. The height distribution of smoke over a fire is determined by the amount of buoyant energy produced by the fire and the amount of energy released by the latent heat of condensation of water vapor. The optical properties of the smoke depend on the size distribution of smoke particles which changes due to coagulation within the lofted plume. This process is slowed by dilution of smoke due to the spreading smoke plume. We present calculations demonstrating these processes and estimate their importance for the smoke source term input for climate models.

Our preliminary calculations based on a standard atmosphere temperature profile show that fires which burn at average rates (e.g., suburban areas with 3 gm/cm^2 of fuel burning for 12 hours) deposit most of their smoke at or below 6 km altitude. Less intense fires (e.g., forested areas with 0.5 gm/cm^2 burning for 12 hours) deposit most of their smoke near 2 km. Only very intense fires, of the Hamburg variety, are able to loft their smoke into the upper troposphere for average atmospheric conditions. These would likely produce a convergent wind pattern that could limit fire spread. The addition of latent heat release by condensation can cause the smoke to spread out at higher altitudes than predicted by a model that does not include condensation. In this case the smoke rises to higher altitudes just above the fire, but returns to lower levels as it spreads, because compensating downward wind currents develop to replenish the upward moving air in the center of the plume.

For high initial smoke densities and for absorbing smoke ($m = 1.75 - 0.3i$), coagulation of smoke particles within the smoke plume is predicted to first increase, then decrease, the size-integrated extinction cross section. However, at the smoke densities predicted in our model (assuming a 3% emission rate for smoke) and for our assumed initial size distribution, the attachment rates for brownian and turbulent collision processes are not fast enough to alter the smoke size distribution enough to significantly change the integrated extinction cross section. Early-time coagulation is, however, fast enough to allow further coagulation, on longer time scales, to act to decrease the extinction cross section. On these longer time scales appropriate to climate models, coagulation can decrease the extinction cross section by almost a factor of two before the smoke becomes well mixed around the globe. This

process has been neglected in past climate effect evaluations, but could have a significant effect, since the extinction cross section enters as an exponential factor in calculating the light attenuation due to smoke.

Introduction

This paper addresses two issues that are crucial for determining the climate effect of massive injections of smoke into the atmosphere: the distribution of the smoke with altitude, and its optical characteristics as determined by coagulation. A very simple "climate" model developed by M. MacCracken can be used to illustrate why these issues are important. Fig. 1 is an illustration of this model. Three levels are defined in the atmosphere. One level is associated with greenhouse gases, one with the smoke cloud, and one with the surface of the earth. The model assumes that a fraction t_c of solar radiation is transmitted through the smoke cloud to the surface of the earth. The fraction α is reflected back to space. As shown in Fig. 1, given fractions of infrared radiation are absorbed and re-emitted by each of the three levels. The fractions of absorbed infrared radiation and reflected and absorbed solar radiation are assumed parameters in this simple model.

Given this framework, an energy-balance equation can be written for each of the three model levels. These three equations can be solved to determine the equilibrium temperature in each of the three layers. The solution for the surface layer temperature, T_s, is given in Fig. 2. The figure also shows the calculated surface temperature for a variety of different assumptions regarding the height of the smoke injection and its infrared and solar optical properties. For illustration purposes, in all cases the albedo, α, is assumed to be constant at zero. With this model, the ambient atmosphere can be approximated by assuming there is no absorption by smoke, ($t_c \approx 0$, $\epsilon \rightarrow 0$), and that the greenhouse gases effectively trap infrared radiation ($\gamma \rightarrow 1$). The model then predicts a surface temperature of 331°. If there were no greenhouse gases ($\gamma \rightarrow 0$), the temperature would drop to the characteristic blackbody temperature of this model system, namely 278°K. The third case considered in Fig. 2 illustrates the effect of assumptions similar to those made by Turco et al. (1983) (hereafter called TTAPS). They considered a baseline case in which the optical depth of smoke in the visible was about 3, so that $t_c \approx 0$. The smoke was distributed throughout the troposphere and into the stratosphere, so that greenhouse gases had little effect ($\gamma \rightarrow 0$). In addition, the smoke was spread throughout the Northern Hemisphere. This meant that the infrared absorption of the smoke (which they estimated as about 1/10 the visible absorption) was small ($\epsilon = 0$). With these assumptions, there is a drastic decrease in T_s to only 234°K, in this model.

The next three cases in Fig. 2 illustrate how the specific assumptions of how the smoke is distributed affect the calculation of T_s, even with massive injections of smoke ($t_c = 0$). If the smoke is at low altitudes, so that greenhouse gases can still trap infrared radiation emitted by the surface layer ($\gamma \rightarrow 1$), the surface temperature might decrease to 308°K, but not nearly so much as in the TTAPS baseline case. If the smoke is not spread so much or, alternatively, if its infrared absorption properties are larger than estimated in TTAPS, then its infrared optical depth may be large enough to effectively trap infrared radiation ($\epsilon \rightarrow 1$). This would cause an increase in T_s, over the case considered by TTAPS to 278°K. In this model the calculated surface temperature for this case, with the smoke above the greenhouse gases, is the same as the effective blackbody temperature of the

SIMPLE EQUILIBRIUM CLIMATE MODEL

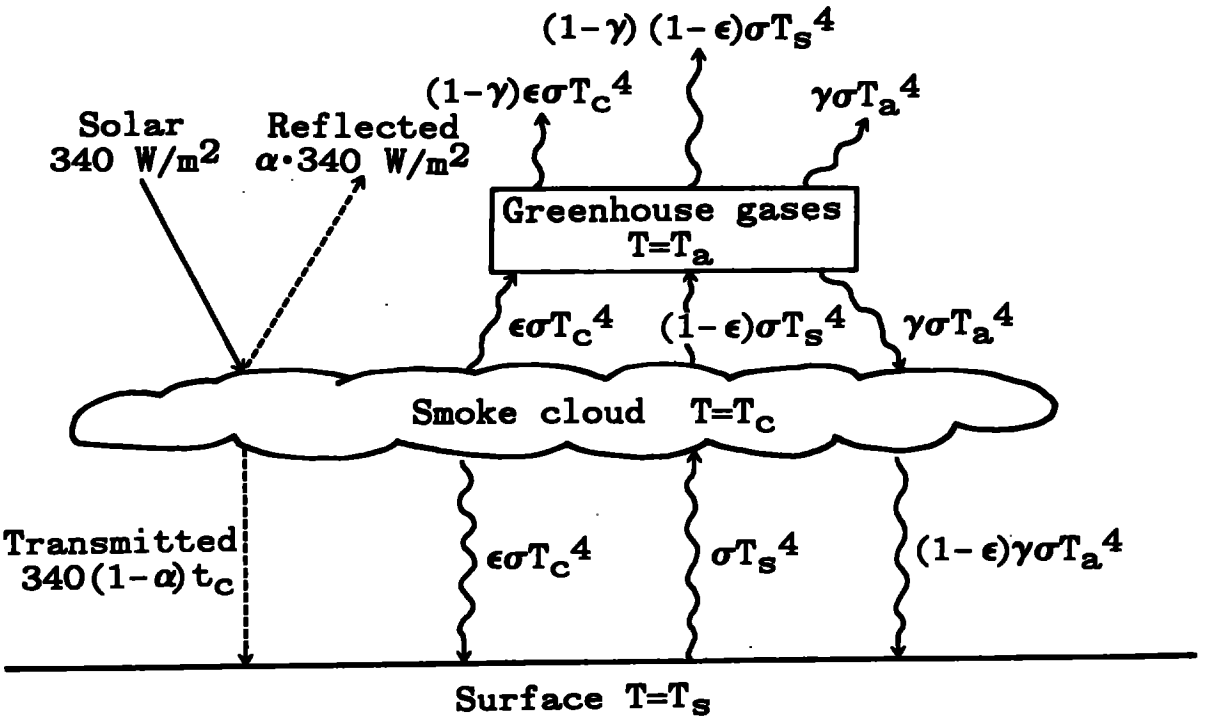

$\sim\sim$ = IR radiation
$=\!=\!=$ = Solar radiation
T_c = Temperature of smoke cloud
T_a = Temperature of atmosphere above smoke cloud
T_s = Surface temperature
α = Albedo
t_c = Fraction of incident solar transmitted through smoke
ϵ = Fraction of incident IR absorbed by smoke
γ = Fraction of incident IR absorbed by greenhouse gases

Figure 1. Illustration of a simple, 3-level equilibrium climate model.

SOLVING THE ENERGY BALANCE EQUATIONS:

Surface temperature:

$$\sigma T_s^4 = 340(1-\alpha)\left[\frac{\gamma}{2-\gamma} + \frac{(1+t_c)}{2-\epsilon}\right]$$

Ambient Atmosphere:	No Smoke (t_c=1; ϵ=0) Absorbing Greenhouse Gases (γ=1)	T_s=331°
Blackbody Temperature:	No Smoke (t_c=1; ϵ=0) No Greenhouse Gases (γ=0)	T_s=278°
Case Considered by TTAPS:	Absorbing Smoke (t_c=0) Small IR Absorption (ϵ=0) No Greenhouse Gases (γ=0)	T_s=234°
Low Altitude Smoke After Spreading:	Absorbing Smoke (t_c=0) Small IR Absorption (ϵ=0) Absorbing Greenhouse Gases (γ=1)	T_s=308°
High Altitude Smoke Before Spreading:	Absorbing Smoke (t_c=0) Large IR Absorption (ϵ=1) No Greenhouse Gases (γ=0)	T_s=278°
Low Altitude Smoke Before Spreading:	Absorbing Smoke (t_c=0) Large IR Absorption (ϵ=1) Absorbing Greenhouse Gases (γ=1)	T_s=331°

Figure 2. Results for the simple, 3-level equilibrium climate model.

earth-atmosphere system. In the last case shown in Fig. 2, if the smoke is at low altitude, below the greenhouse gases, the calculated surface temperature is the same as that in the ambient atmosphere, namely 331°K.

This simple model shows that in order to predict the climate effects of a given amount of smoke, it is necessary to know the distribution of the smoke with altitude. In addition the solar and infrared optical properties of the smoke (which affects t_c and ϵ) must be known.

This paper will discuss a calculation of the height distribution of smoke above fires and the optical properties as determined by coagulation processes in the smoke plume.

Height Distribution of Smoke

We have calculated the height distribution of smoke with a model that was first developed to describe hydrodynamic flows within an internal combustion engine (Haselman, 1980). The calculations shown here were developed using a slab (or two-dimensional) model configuration. The calculations assume a line fire of 10 km width and infinite extent. Average atmospheric conditions were assumed (see Penner et al., 1985).

Figure 3 shows the velocity field that develops with an energy source similar to that which would be predicted if the TTAPS forest fuel loading of 0.5 gm/cm^2 were burned in about 12 hours time. The figure shows that winds are perturbed from the ground to around 2 km altitude. Smoke mass mixing ratio contours for this fire are shown in Fig. 4. These are mass mixing ratio contours, rather than density contours; the figure shows that more than 50% of the smoke from this fire would be injected below 2 km altitude (see Penner et al., (1985) for smoke mixing ratio values).

Figure 5 shows the velocity field from a slightly more intense fire. This energy source is consistent with burning an average fuel loading of 3 g/cm^2 in about 12 hours. Velocities are perturbed up to about 4 km altitude, and the smoke spreads out between 3-1/2 and 4 km (see Fig. 6).

All of the calculations to this point have considered only a quiescent, dry atmosphere. However, if water vapor is swept into the convection column and condenses at high altitude, the latent heat of condensation may add significant energy to the smoke plume and raise the level of injection. As shown in Fig. 6, in this mid-energy case, the smoke is deposited some 2 to 3 km higher than if the atmosphere were dry and no condensation occurred.

Figure 7 shows the velocity field for a high intensity fire. The energy source for this fire is equivalent to that which might be produced if 10 gm/cm^2 of fuel burned in 6 hours. In this case, windfields are perturbed up to the tropopause (at 11.5 km), but there is a tendency for the smoke to settle and spread out at somewhat lower levels (see Fig. 8), between 7 and 8 km. If water vapor is carried to altitude with the convection column, the smoke level above the fire is raised, by about 2 km (see Fig. 9).

The amount of water that is condensed in the high intensity fire is roughly 2 or 3 times that required to form rain in the ambient atmosphere. This raises the possibility that, at early times in intense fires, much of the smoke could be removed rapidly by precipitation created in the upper part of the convection column.

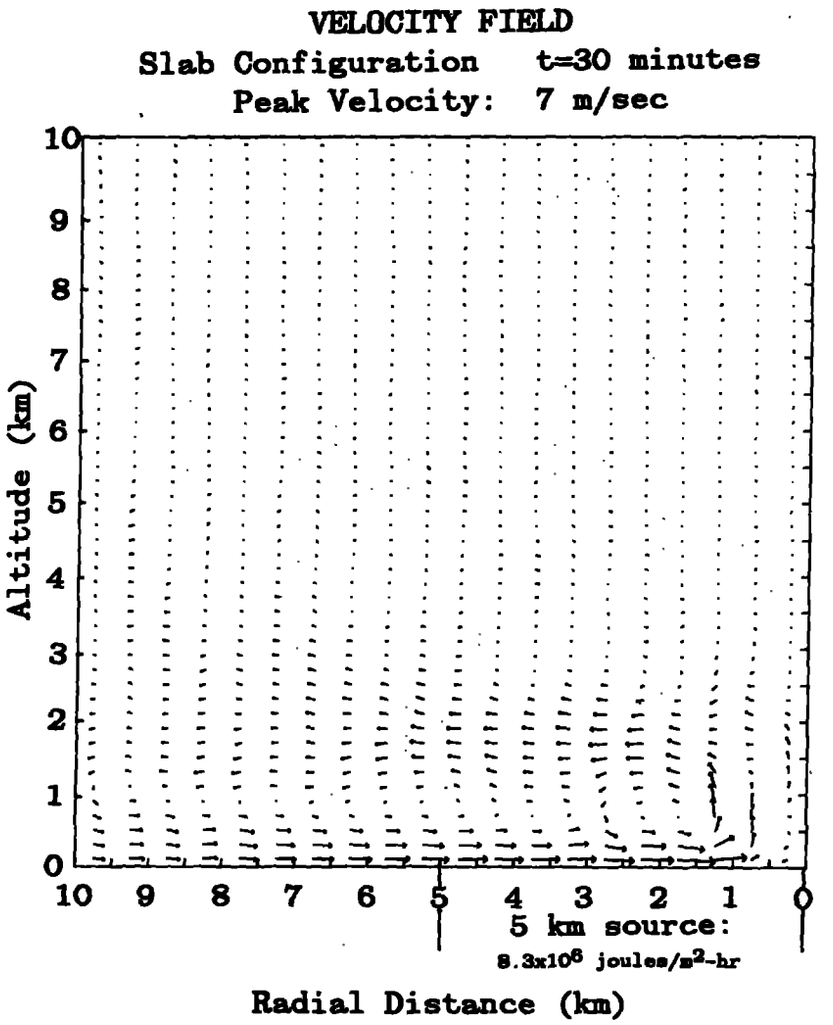

Figure 3. Velocity field after 30 minutes for an energy source of intensity $8.3 \times 10^6 J/m^2$-hr. The maximum velocity is 7 m/sec.

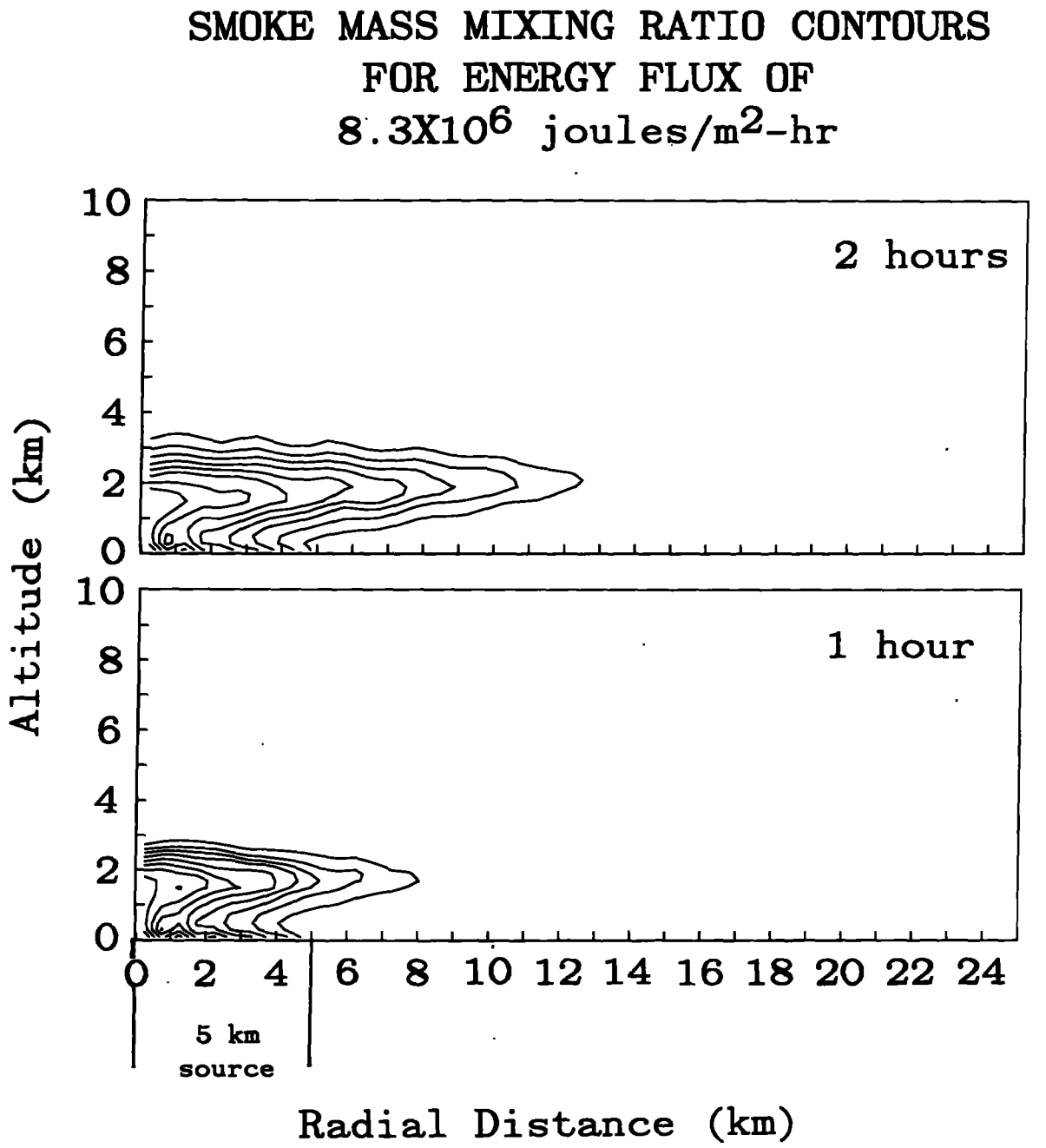

Figure 4. Smoke mass mixing ratio contours after 1 hour and 2 hours for an energy flux of 8.3×10^6 J/m^2-hr.

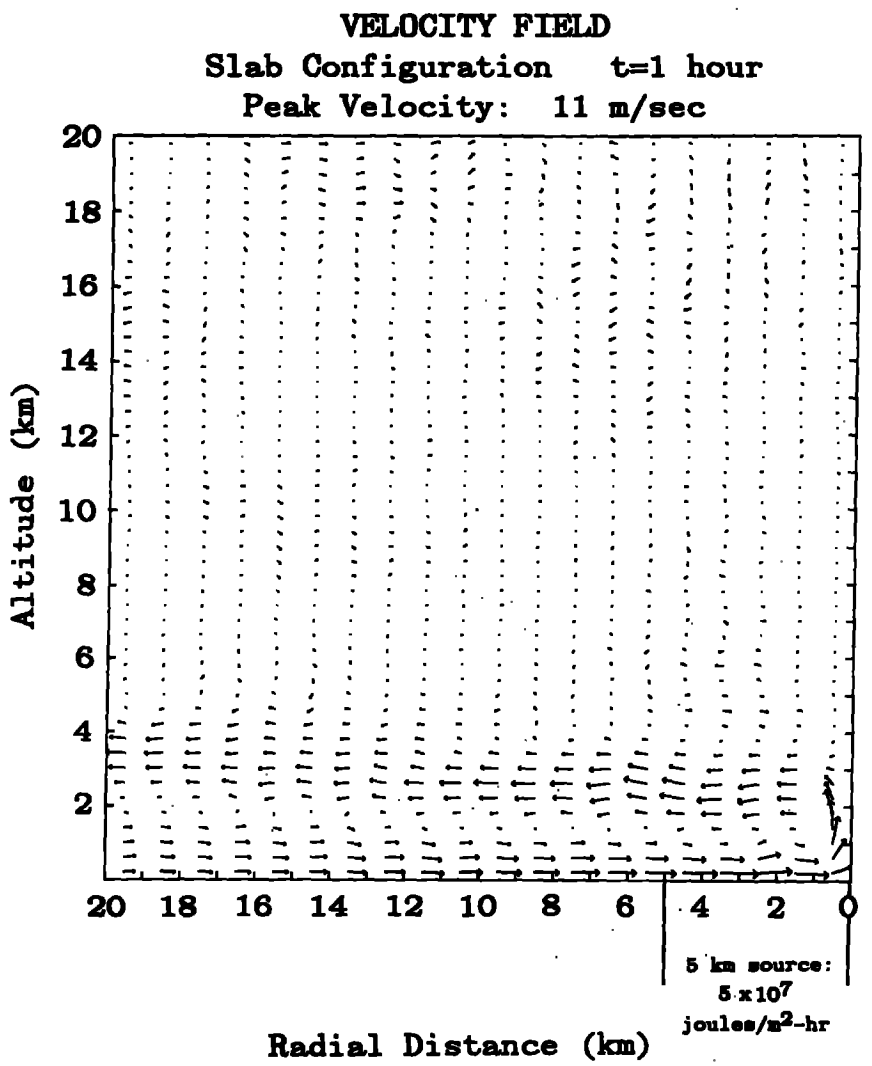

Figure 5. Velocity field after 1 hour for an energy flux of 5×10^7 J/m^2-hr. The maximum velocity is 11 m/sec.

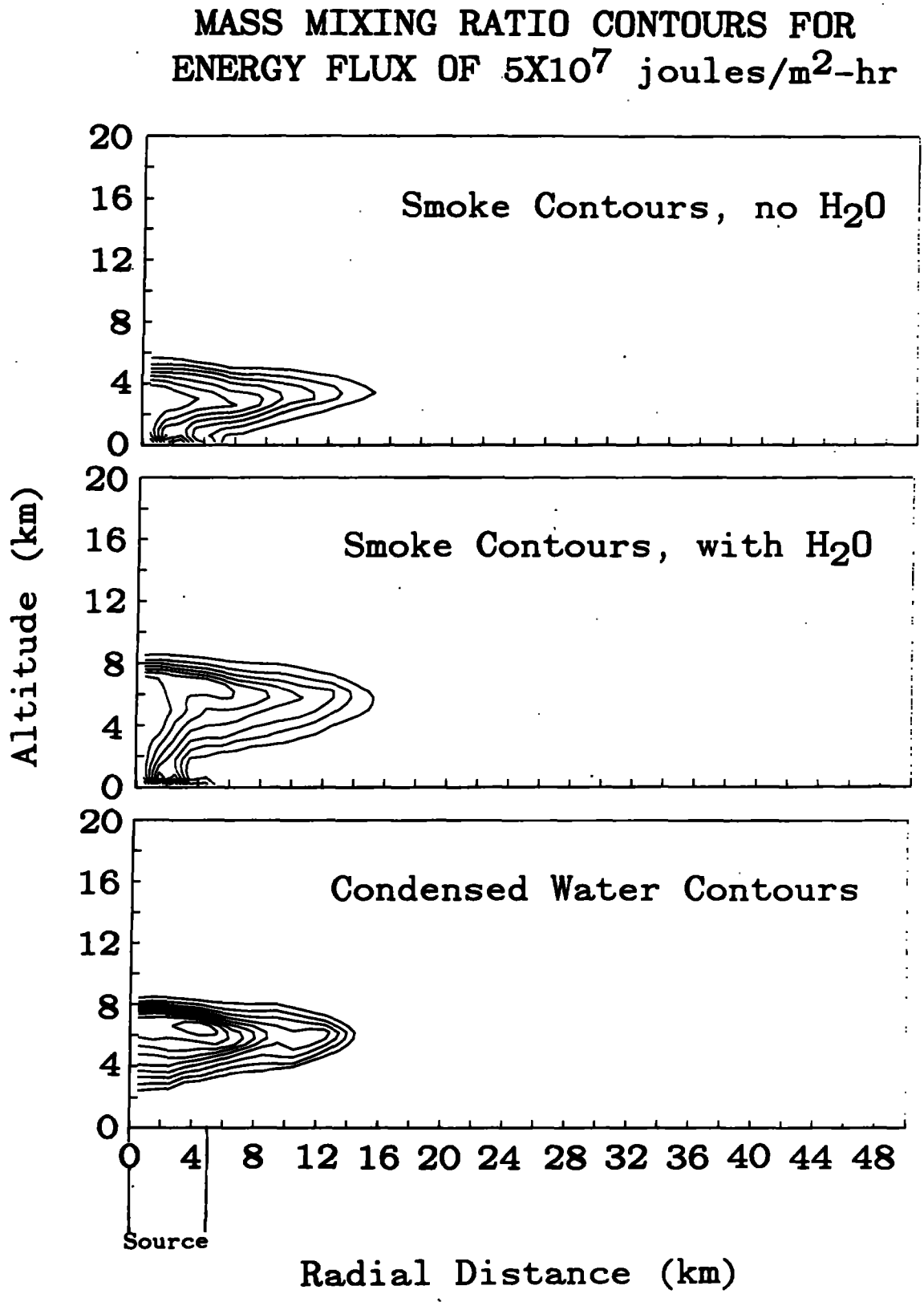

Figure 6. Smoke and condensed water mass mixing ratio contours for an energy flux of 5×10^7 J/m²-hr. The top graph illustrates the smoke contours generated for a dry atmosphere in which H_2O does not condense. The middle graph shows smoke contours if H_2O does condense, and the lower graph shows the condensed water contours for this case.

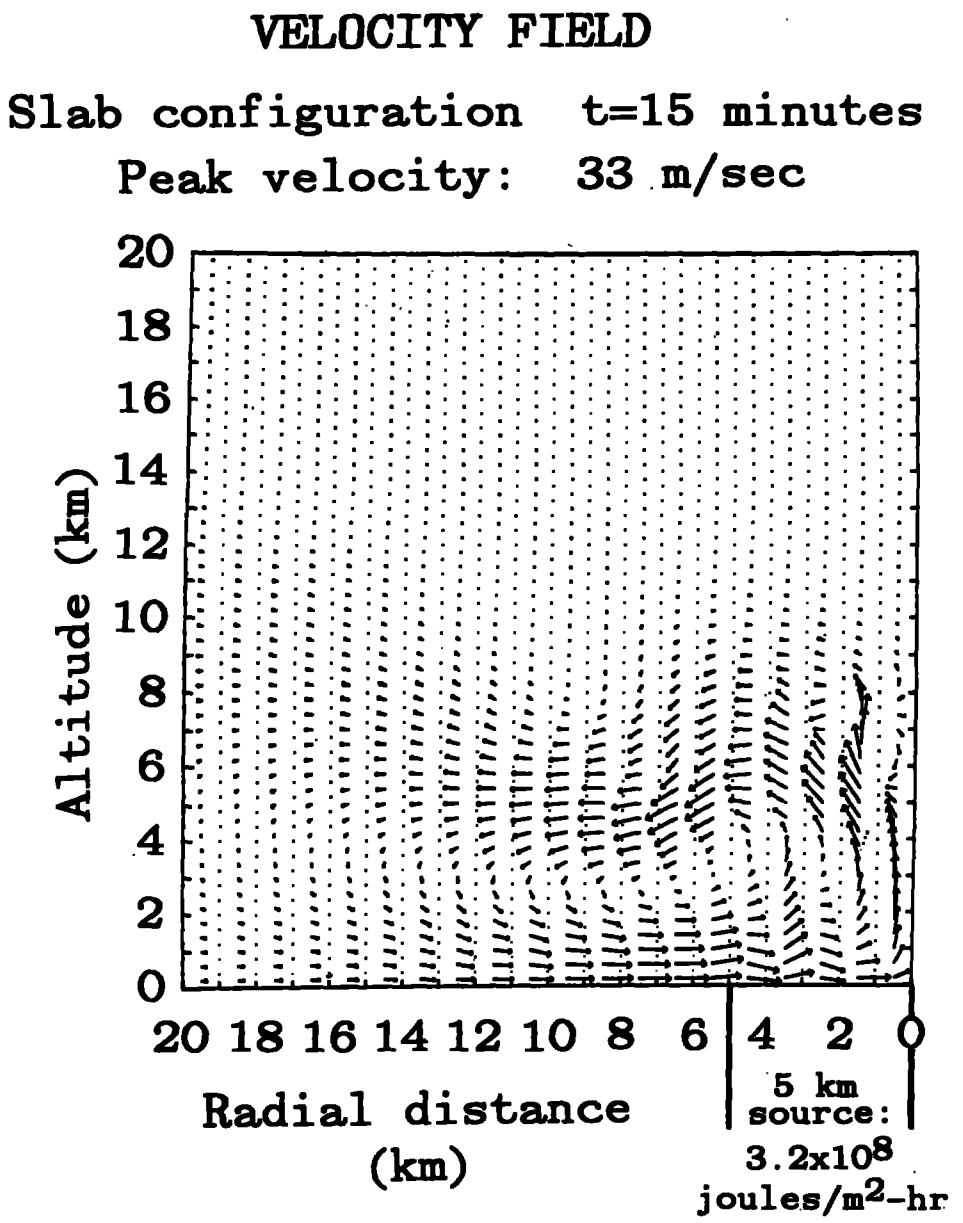

Figure 7. Velocity field after 15 minutes for an energy flux of 3.2×10^8 J/m^2-hr. The maximum velocity is 33 m/sec.

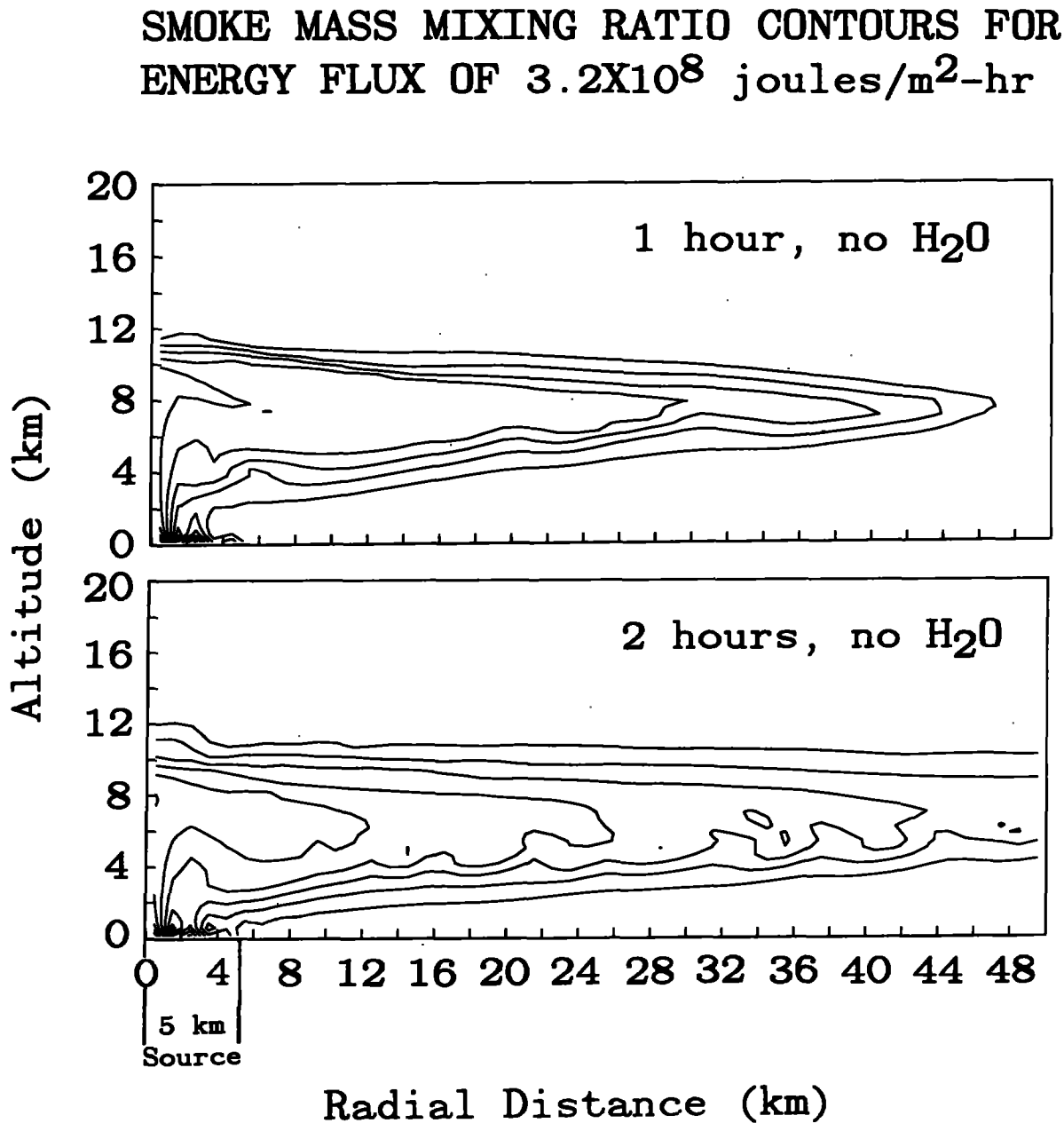

Figure 8. Smoke mass mixing ratio contours after 1 hour and 2 hours for an energy flux of 3.2×10^8 J/m^2-hr. Water vapor was not allowed to condense in these calculations.

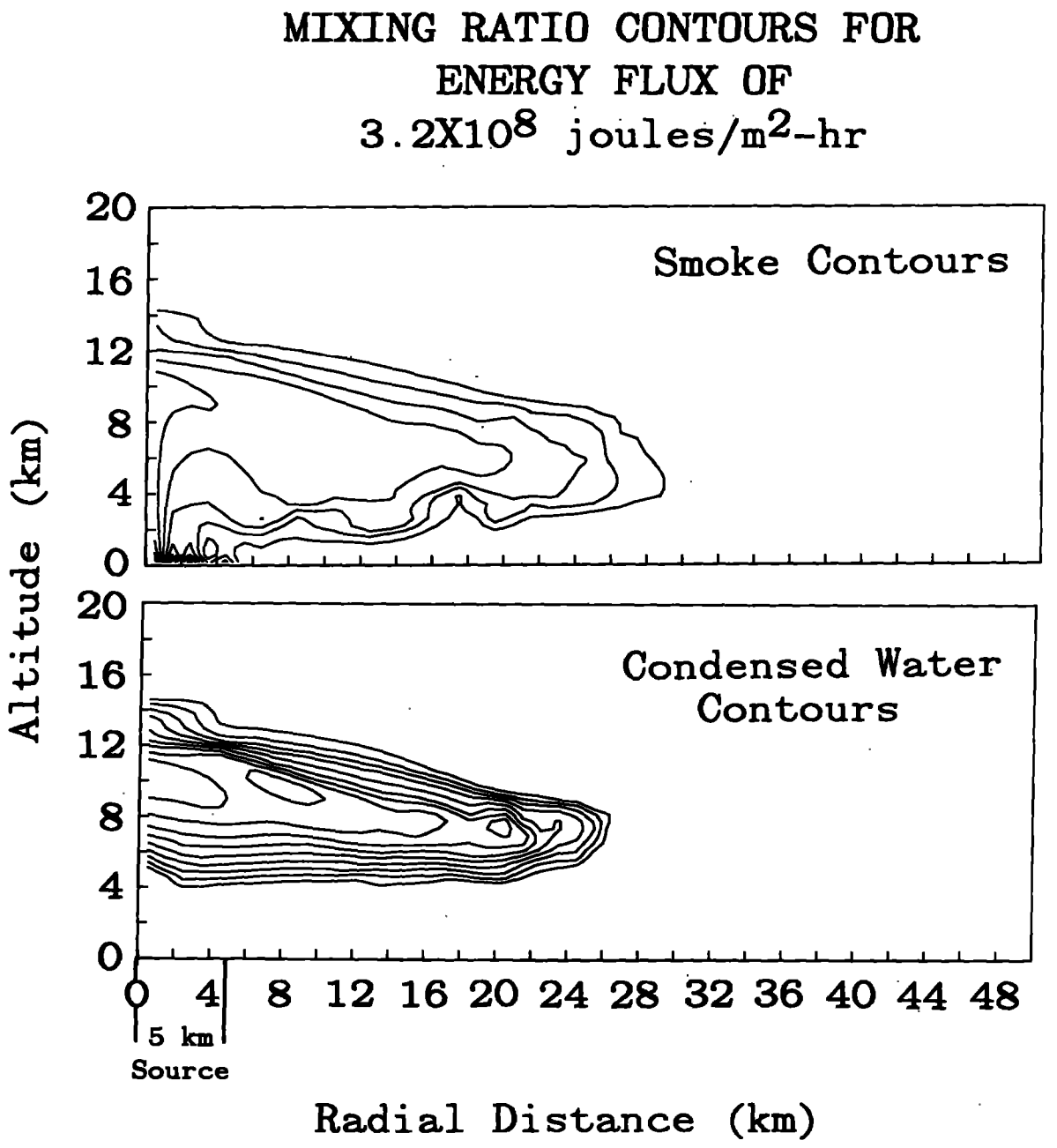

Figure 9. Smoke and condensed water mass mixing ratio contours after 1 hour for an energy flux of 3.2×10^8 J/m^2-hr. In contrast to the calculation shown in Fig. 8, water vapor was allowed to condense for this calculation.

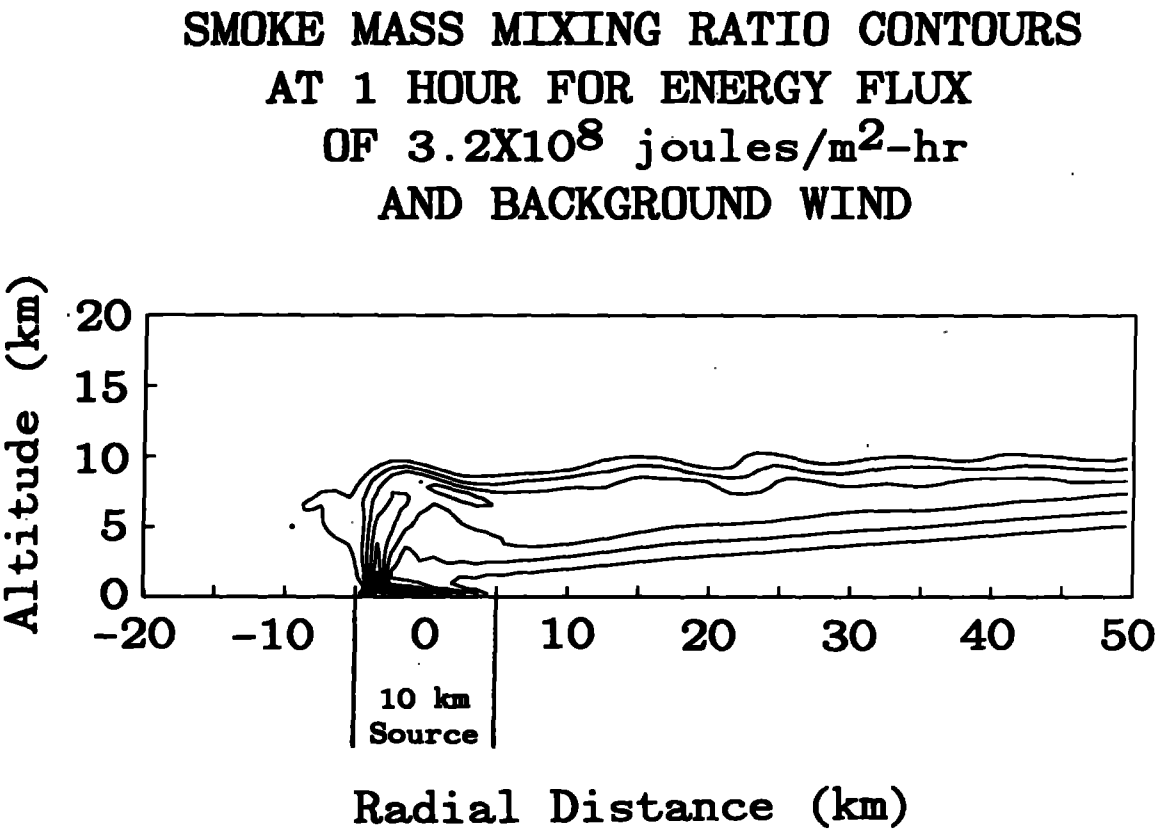

Figure 10. Smoke mass mixing ratio contours after 1 hour for an energy flux of 3.2×10^8 J/m^2-hr when an average background wind including vertical shear is assumed present.

Finally, Figure 10 shows how the presence of a background wind alters the smoke injection height. Here, a background wind with magnitude 2 m/sec at the surface increasing linearly to 20 m/sec at the tropopause was imposed. In this calculation, the presence of the background wind appears to increase slightly the level of smoke injection, from 7 or 8 km to 8 or 8.5 km.

In summary, these sample calculations show that the height of deposition of smoke above a large-area fire depends on the meteorological conditions present during the fire as well as the fire intensity. Further analysis with this model and with a 3-D version of this model supports the preliminary calculations presented here (see Penner et al., 1985). Specifically, our results are not consistent with large amounts of smoke entering the stratosphere even with a very intense fire. This conclusion results, in part, from our use of average meteorological conditions for relative humidity, temperature, and background winds. For special meteorological conditions, of course, a larger fraction of smoke may reach levels above the tropopause (see Cotton, 1985). But, since much of this smoke is returned to the troposphere by downward sloping wind fields, as the fire continues to burn, a smaller fraction of the total remains at the highest altitude. As mentioned above, further study, with models capable of simulating the detailed microphysical processes describing the scavenging of smoke by precipitation, is needed to determine the ultimate fate of the smoke. In addition, on longer time scales, solar absorption, with the resultant heating and lifting of the smoke layer itself, must also be considered.

Coagulation and Optical Properties of Smoke

Figure 11 illustrates how the size distribution and index of refraction of smoke determine its extinction coefficient. The extinction cross section per gram of smoke is plotted for a log-normal size distribution as a function of the mode diameter, d. The curves marked $\sigma = 2.0$ have a particle distribution that is distributed more widely about the mode diameter than those with $\sigma = 1.5$. Smoke particles with refractive index $m = 1.75 - 0.3i$ are more highly absorbing* than those with $m = 1.5 - .001i$ which are almost entirely scattering.

Particles form within flames at very small sizes, with $d \approx .002\mu$m. As they leave the flame, these particles grow through processes of coagulation and condensation. Fig. 11 shows that if they are distributed with $\sigma = 2.0$, their extinction cross section increases up to a maximum value of about 10 m^2/g, when their mode diameter is about $0.03\mu m$. Further coagulation and growth of the particles then starts to decrease their extinction cross section. The extinction cross section for a narrower distribution, represented by the curve $\sigma = 1.5$, peaks at somewhat larger mode diameters, near 0.1 μm.

Figure 11 also shows the cross sections which result from the assumptions made by TTAPS for nonurban (or forest) smoke and for urban smoke. Recent measurements by Patterson and McMahon (1984) of the smoke associated with forest fuels are not consistent with the assumption made by TTAPS. Patterson and McMahon find a specific absorption extinction coefficient for forest fuel smoke of only 1 m^2/gm under flaming conditions. As

* For $m = 1.75 - 0.3i$, the single scatter albedo is about 0.5 as long as mode radius is larger than about $0.1\mu m$.

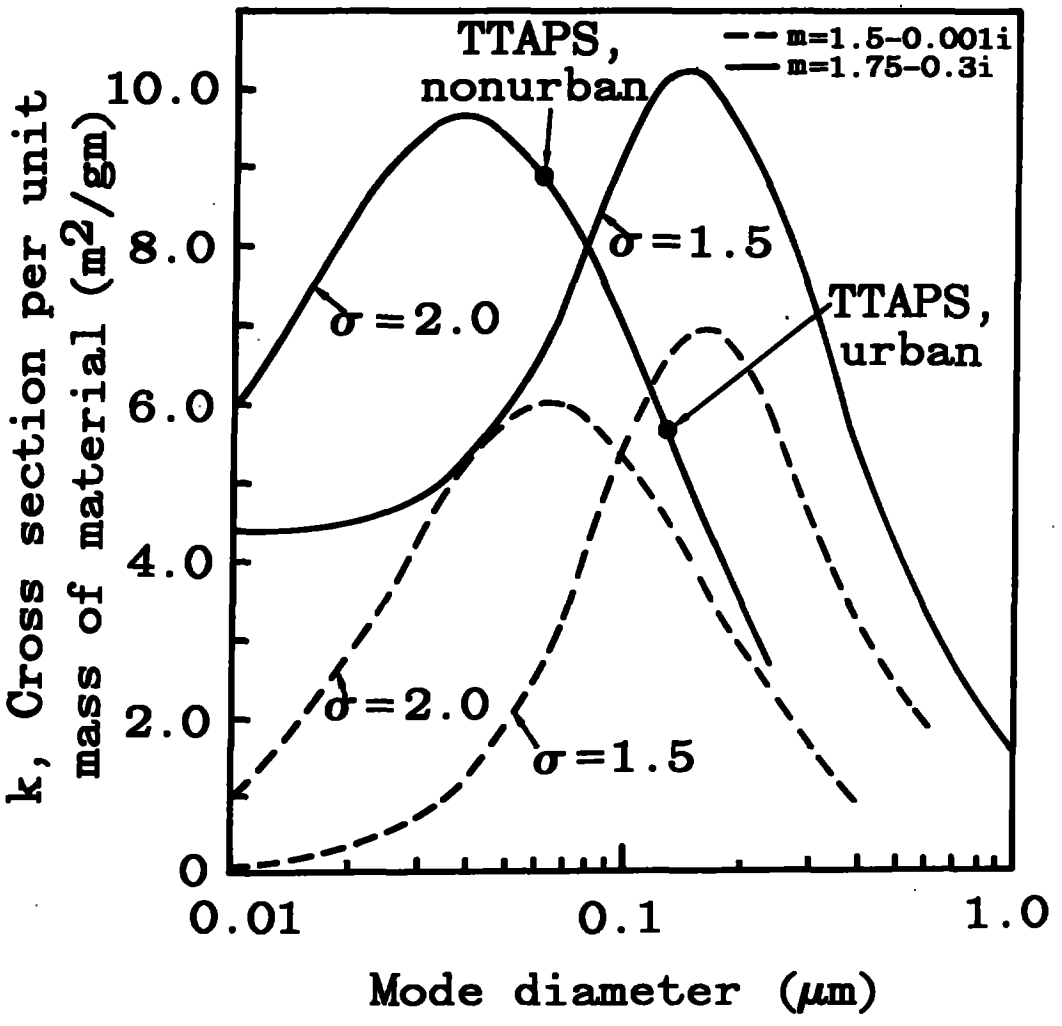

Figure 11. Extinction cross section per unit mass of smoke as a function of the mode diameter of a log-normal size distribution. Dashed curves were calculated assuming a refractive index (m) of 1.5–0.001 *i*. Solid curves were calculated assuming a refractive index of 1.75–0.3 *i*. For each refractive index two curves are shown illustrating the variation of the extinction cross section with the mode diameter of a log normal distribution whose standard deviation (σ) is 1.5 and 2.0.

shown in Fig. 11 the TTAPS absorption coefficient is four times larger, given a single scatter albedo of 0.5. In addition, Patterson and McMahon used a previously established size distribution to infer a refractive index of $1.5 - 0.05i$. If these measurements are representative, forest fire smoke will play a much smaller role in determining the climate impact of a nuclear war than was estimated by TTAPS.

Figures 12 and 13 illustrate how coagulation might affect an initial large particle size distribution, with mean geometric radius, r_g, of 0.1μm and an initial small particle size distribution with r_g of 0.01μm, respectively. The size distributions in both figures were calculated assuming initial loadings of 2×10^{-7} gm/cm^2. This density of smoke is characteristic of that which is typically measured within flames (Bard and Pagni, 1981), but is higher than smoke densities measured over experimental fires (Ward, 1984). The initial number densities of smoke particles in these figures are 5.5×10^6/cm^3 and 5.5×10^9/cm^3, respectively. Since the rate of coagulation is proportional to the number of particles squared, coagulation proceeds much more rapidly for the distribution with the smaller mean geometric radius. However, after one hour, both distributions reach similar number concentrations, namely 5.2×10^5/cm^3 and 6.6×10^5/cm^3, respectively. The smaller size initial distribution is more narrow and has more particles near 0.1 μm than the distribution with an initial mean geometric radius of 0.1 μm. We would expect, therefore, that the smaller initial distribution should result in a larger extinction cross section after significant amounts of coagulation.

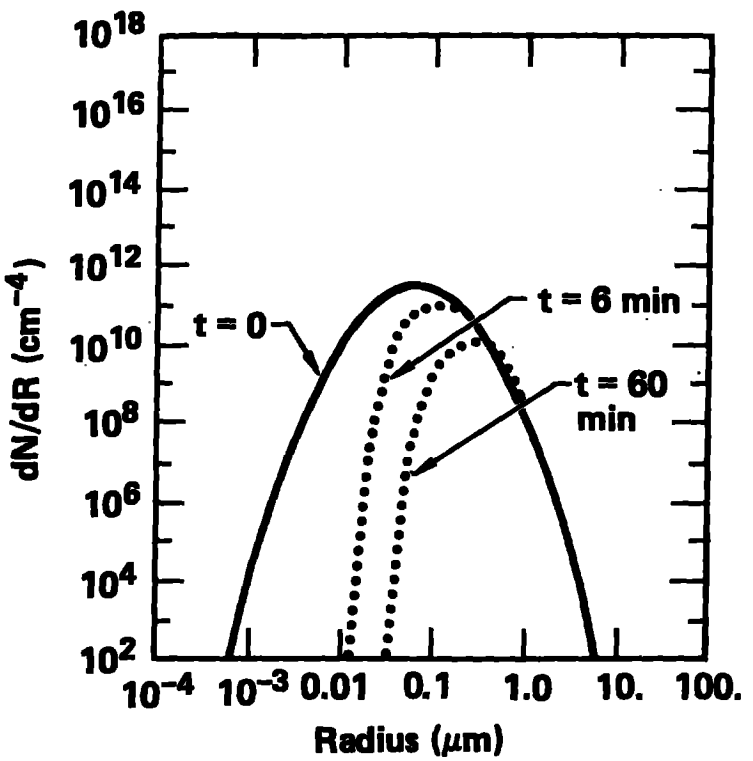

Figure 12. Evolution of a log-normal size distribution function with mean geometric radius of 0.1 μm and standard deviation of 2.0. The initial smoke density was 2.0×10^{-7} g/cm^3. This is equivalent to an initial number concentration of 5.5×10^6 g/cm^3.

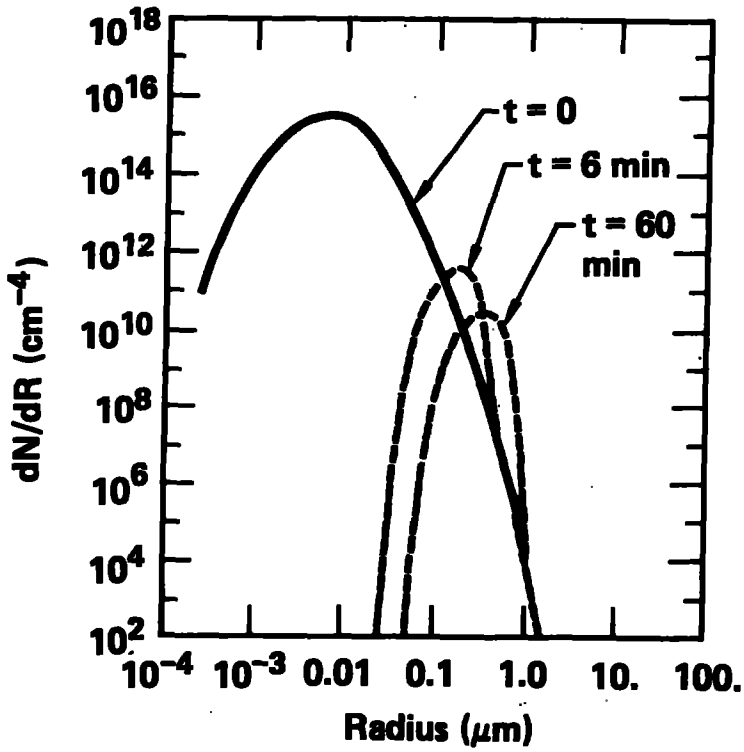

Figure 13. Evolution of a log-normal size distribution function with mean geometric radius of 0.01 μm and standard deviation of 2.0. The initial smoke density was 2.0×10^{-7} g/cm^3. This is equivalent to an initial number concentration of 5.5×10^9 g/cm^3

Fig. 14 illustrates how the extinction cross section changes with time due to the process of coagulation. In addition to the initial size distributions considered in Figs. 12 and 13, the extinction cross section for an intermediate distribution is shown ($r_g = 0.05$ μm) as well as one typical of distributions measured within a flame produced by burning wood (Bard and Pagni, 1981). Figure 14 illustrates that, if coagulation is the only process affecting smoke concentration, the resulting cross section (for this refractive index) will lie between 3 and 5 m^2/g, independent of the initial distribution.

Unfortunately, coagulation is not the only process affecting the evolution of the size distribution. Dilution and spreading of the smoke plume can decrease smoke concentrations, thereby "freezing" the coagulation process. Figure 15 shows how dilution of the smoke plume changes the evolution of the cross section for an initial distribution with $r_g = 0.01$ and $\sigma = 2.0$. For this calculation the total density of smoke was decreased from an initial concentration 2×10^{-7}g/cm^3 at a rate proportional to $1/\tau_d$, where τ_d is the assumed time constant for dilution. Cases with $\tau_d = 360$ sec, 3600 sec and $\tau_d = \infty$ (no dilution) are shown. For relatively rapid dilution, ($\tau_d = 360$ sec), the process of coagulation is "frozen" early in the calculation, and the resulting cross section after one hour remains near its initial value. Likewise, if the initial smoke density is smaller than values typically measured within flames, the initial number density will be small and coagulation will not be as fast (see curve labeled 2×10^{-9}g/cm^3). We may conclude that if dilution is rapid, the initial size distribution will be an important parameter for determining the

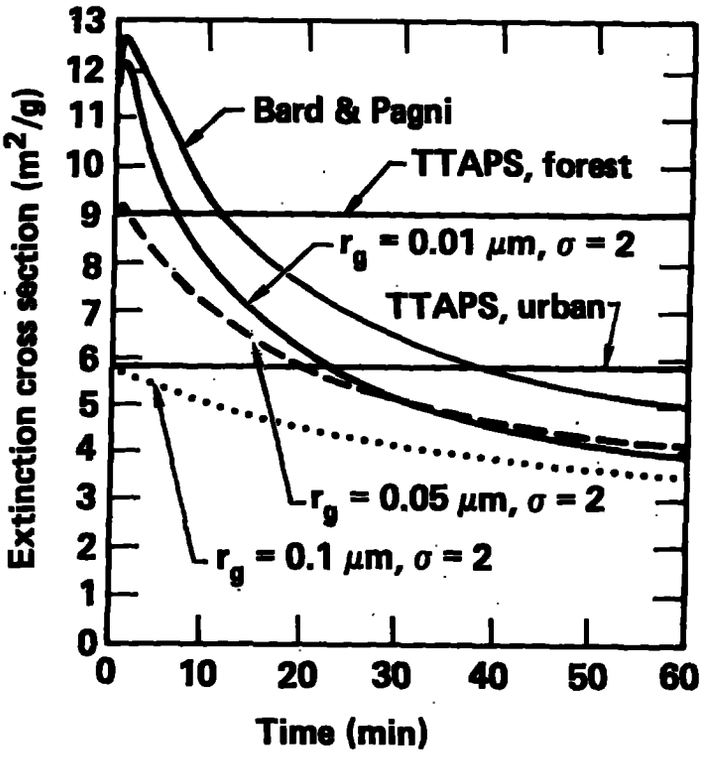

*Assumes refractive index = 1.75 – 0.3i and initial concentration = 2.0×10^{-7} gm/cm^3

Figure 14. Evolution of the extinction cross section due to coagulation for several initial size distributions. In each case the density of smoke was 2.0×10^{-7} g/cm^3 and the refractive index was 1.75–0.3 i.

optical characteristics of the smoke. The initial size distribution ideally should be determined from measurements. Unfortunately, the size distribution appropriate to a raging urban fire is not easily determined. It is probable that the fire will involve some regions in which smoldering combustion takes place, and some in which flaming combustion occurs. The burning fuels from an urban fire will include a variety of modern plastics and other synthetics, as well as wood. Figures 16 and 17 show measured size distributions of smoke produced in laboratory tests of the combustion of a variety of fuels under smoldering and flaming conditions (Bankston et al., 1978). As shown by comparing these figures, the measured mean geometric radius for smoke produced under smoldering conditions is generally larger than that for smoke produced under flaming conditions. Thus if we assume a characteristic composition such that the refractive index is $1.75 - 0.3i$*, we calculate extinction coefficients for smoke from the smoldering materials shown in Fig. 16 ranging from 1.7 to 6.0 m^2/g. For smoke produced under flaming conditions, the calculated range for the materials shown in Fig. 17 is 8.3 to 8.8 m^2/g. Since the smoke produced under flaming conditions should contain more elemental carbon per unit mass than that produced by

* Smoke produced under smoldering conditions, is generally "whiter" than that produced under flaming conditions, at least for forest fuels. Also, smoke from different fuels should have varying absorptive properties. Thus the assumption of constant refractive index for smoldering and flaming combustion and all fuels is poor, but here we simply want to isolate the effects of size.

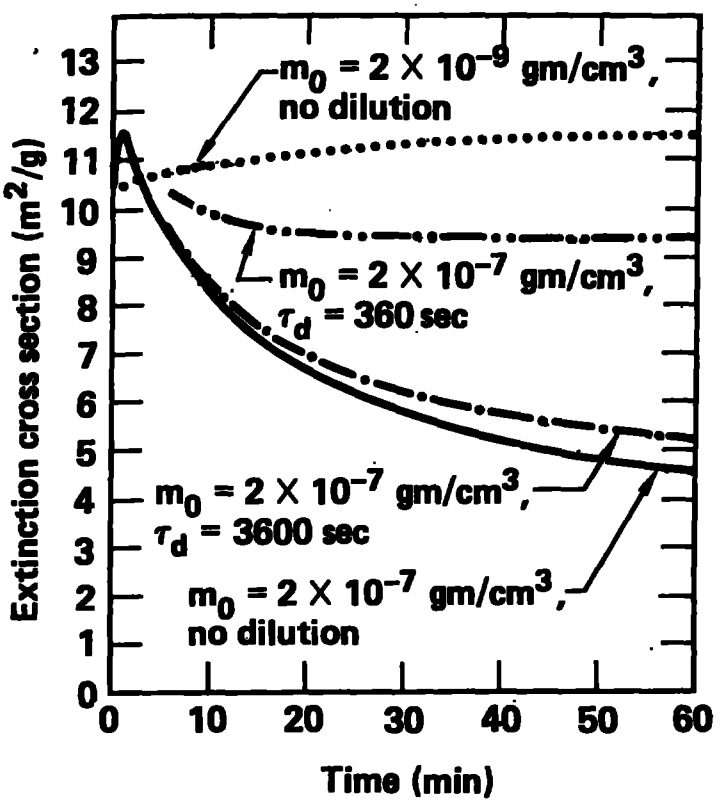

Figure 15. Evolution of the extinction cross section due to coagulation when the density of smoke is continuously diluted by mixing with clean background air. Several initial densities of smoke and dilution time constants are shown.

smoldering, these smokes should in general have higher extinction cross sections due to their more absorbing composition as well as due to their smaller size. However, the emission rates for smoke produced under flaming conditions are lower than the emission rates for smoldering combustion. For example, Bankston et al. (1978) found that the quantity of smoke released from one experiment with wood was below their detection limit, implying emission rates of less than 1% under some flaming conditions. For the same external conditions but with smoldering combustion the emission rate for wood was 15.4%. Therefore, in order to use these data to determine initial smoke production rates and optical characteristics, the relative amounts of different fuels available to burn must be estimated. Also the amount burned under the various conditions of temperature, external radiation, etc. must be determined.

Since this task is beyond the scope of the present study, we have rather arbitrarily chosen an initial size distribution characteristic of forest fire fuels (Patterson and McMahon, 1984), namely a log-normal distribution with $r_g = 0.045$ and $\sigma = 1.75$. In addition, we have assumed a refractive index of $1.75 - 0.3i$ in order to be consistent with the value assumed by TTAPS.

Estimation of Initial Smoke Density and Dilution in Plume

As discussed above, the importance of coagulation depends on both the assumed initial size distribution and the initial smoke density. The density of smoke within a flame is close

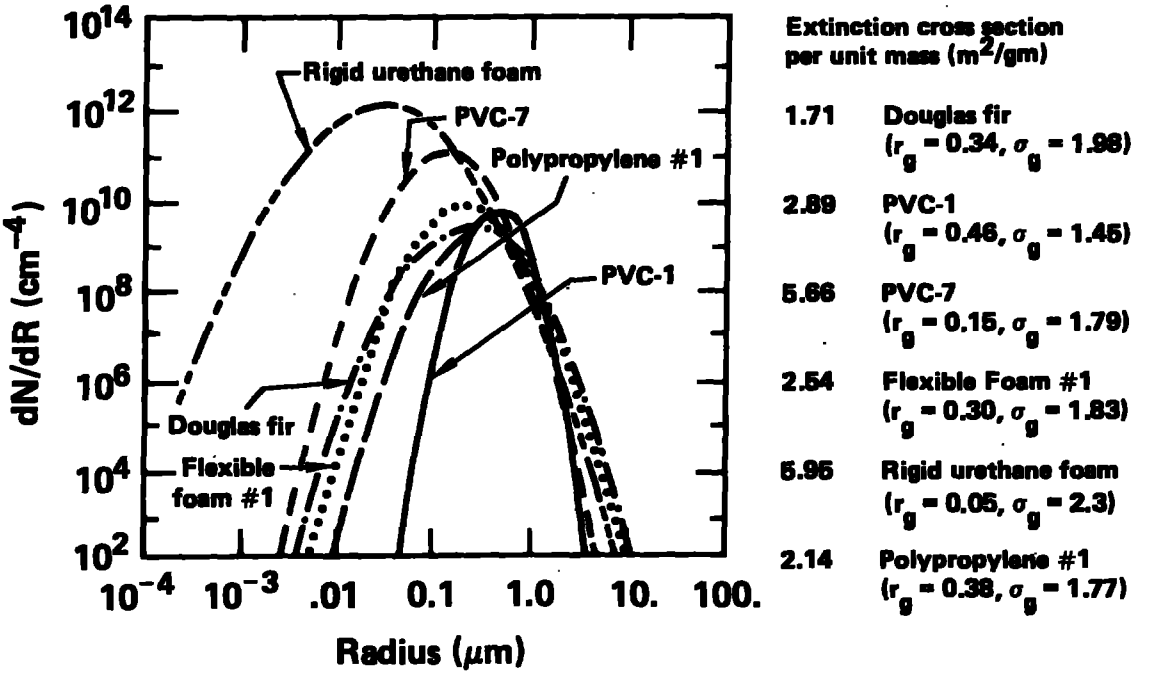

*Extinction cross section was calculated assuming a refractive index of 1.75 – 0.3i and mass loading of 2.0×10^{-7} gm/cm^3

Figure 16. Size distributions for smoke produced under smoldering or nonflaming conditions for a variety of materials. Extinction cross sections were calculated assuming a refractive index of 1.75–0.3 i.

to 2×10^{-7}g/cm^3, but, as the smoke leaves the flame, it can decrease in mass and size due to oxidation to gaseous form or it can increase in mass and size due to condensation of low vapor pressure gases. Therefore, for our calculations, we need some independent method for estimating the density and size distribution of smoke, appropriate to some volume excluding the flame itself. Again, given the lack of measured concentrations and densities near major fires, we have instead used the maximum concentration calculated in our model of the dynamics associated with large scale fires. If we assume a smoke emission rate of 3%, we calculate an initial smoke density of 5×10^{-8} g/cm^3 directly above the fire. This density is, incidently, consistent with the densities measured at a height of approximately 15 m above experimental fires of forest fuels (Ward, 1984).

To calculate how dilution affects the evolution of the size distribution, we estimated the decrease in smoke mass per unit time by calculating a dilution time constant from our calculations of the dynamics associated with large scale fires. In particular, let x_1 be the density of a parcel of smoke at time t located at position $\vec{r}_1$. If, in the time interval between t_1 and $t_1 + \Delta t$, the parcel moves to location $\vec{r}_2$ and has a density at this location of x_2, then the dilution time constant for this time interval is taken as

$$\tau_d^{-1} = -\frac{x_2 - x_1}{x_1 \Delta t} \qquad (1)$$

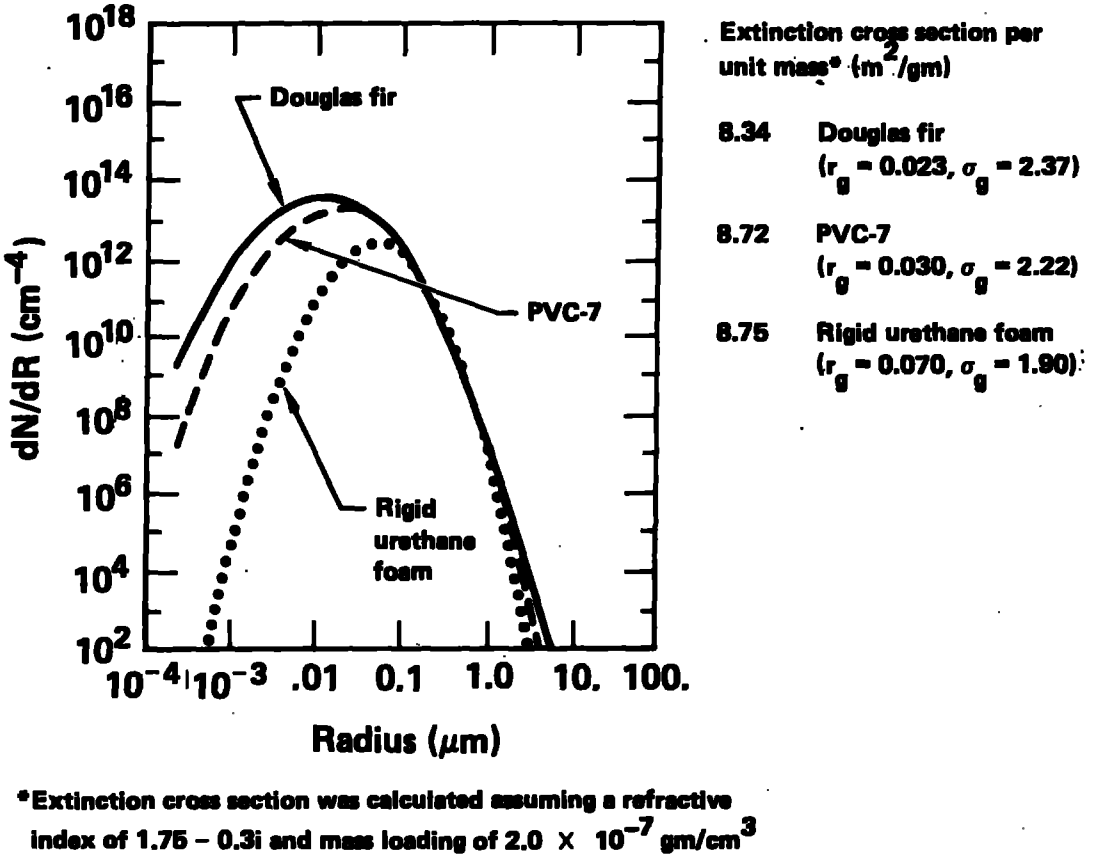

Figure 17. Size distributions for smoke produced under flaming conditions for 3 different materials. The extinction cross sections were calculated assuming a refractive index of 1.75–0.3 *i*.

Smoke particle concentrations are then decreased according to

$$\frac{\partial n(r)}{\partial t} = -\frac{n(r)}{\tau_d}. \qquad (2)$$

Using this formulation, we can calculate how dilution and coagulation simultaneously affect the size distribution and optical characteristics of a parcel of smoke that begins above the fire and is lofted to altitude along some trajectory within the smoke plume. Figure 18 shows the evolution of the size distribution during the first hour within the smoke plume from such a calculation. Small smoke particles are rapidly decreased by attachment to larger ones. The calculated extinction coefficient grows from an initial value of 10.5m^2/g to 11.6m^2/g as particles first move into sizes that more effectively interact with light. Then it begins to decrease as the majority of particles become larger and therefore interact less effectively with light.

After 1 hour, the extinction cross section is 9.3 m^2/g, close to the assumed initial value. The effects of coagulation should continue, of course, as the smoke spreads further downwind of the fire. Depending on how quickly the smoke plume is diluted, this longer time scale coagulation may or may not further decrease the extinction coefficient. To estimate the importance of coagulation in global scale models, we developed a dilution

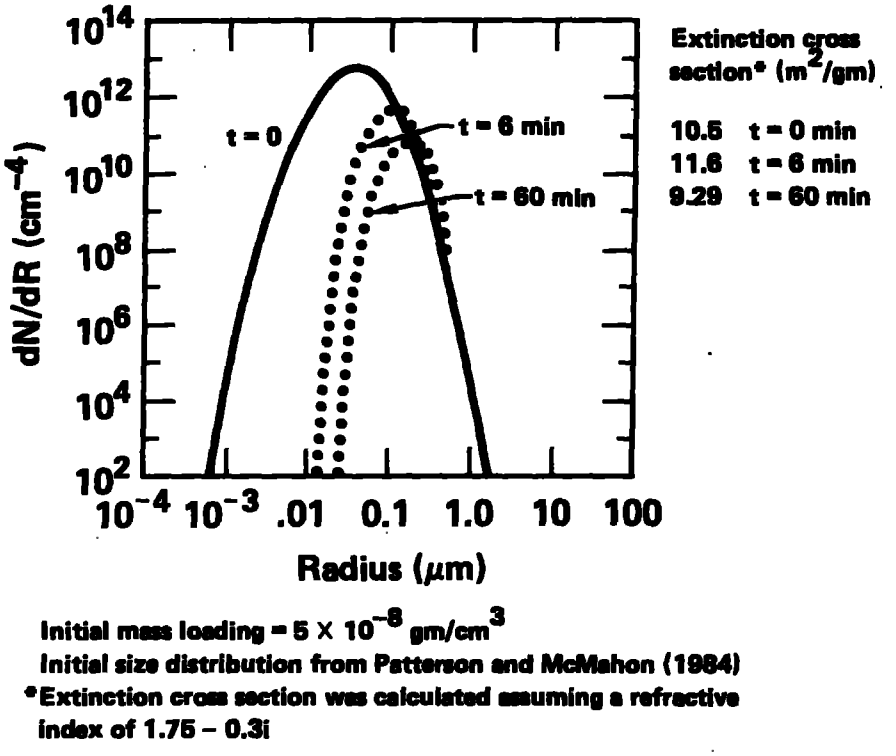

Figure 18. Effect of coagulation on aerosol size distribution within the urban smoke plume. The initial mass loading of smoke was 5.0×10^{-8} g/cm^3. The initial size distribution was log-normal with $r_g = 0.045$ and $\sigma = 1.75$. Extinction cross sections were calculated assuming a refractive index of 1.75–0.3 i.

time constant for the first 30 days of smoke spreading with trajectories as estimated from the model of MacCracken and Walton (1984). For this calculation, the initial smoke density was assumed to be 8×10^{-10}gm/cm^2, consistent with densities calculated in the MacCracken and Walton model. The initial size distribution assumed by Turco et al. (1983) for smoke from urban fires was used (i.e., $r_g = 0.1$ μm, $\sigma = 2$). Figures 19 and 20 show how this size distribution and its extinction coefficient change with time as coagulation proceeds within the global-scale smoke plume. Coagulation decreases the visible cross section of the smoke by 40% in the first week but appears to be "frozen" after that time. Since the amount of light attenuation by smoke is exponentially dependent on the extinction cross section a decrease of 40% is clearly important. Therefore coagulation should be accounted for in calculations of the climate effect of massive amounts of smoke.

Summary

Preliminary calculations with a slab configuration model indicate that only very intense fires, equivalent to those expected when city centers burn, will loft smoke into the upper troposphere. Further, under the meteorological conditions considered here, very little of this smoke is injected into the stratosphere.

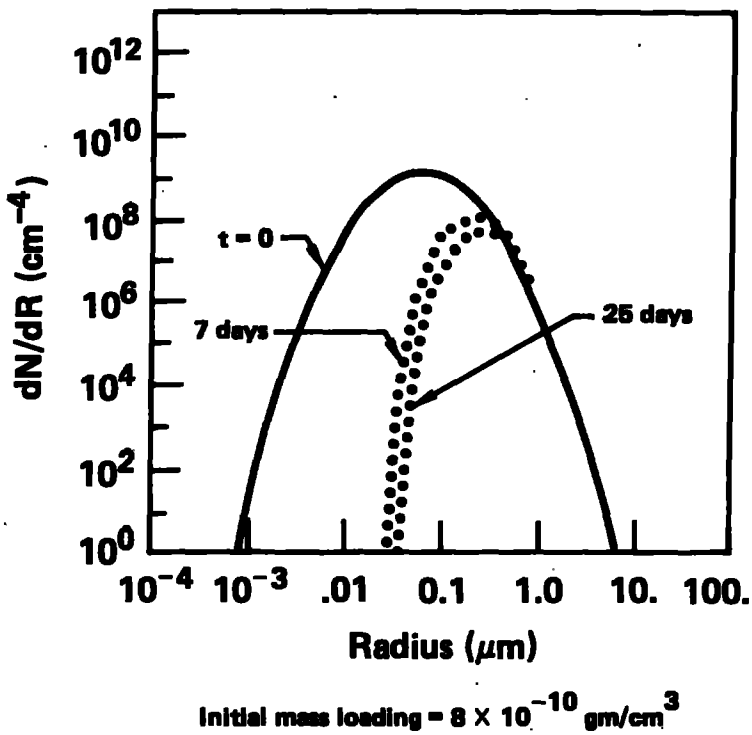

Figure 19. Effect of coagulation on the aerosol size distribution within the global smoke plume. The initial mass loading of smoke was 8.0×10^{-10} g/cm^3. The initial size distribution was log-normal with $r_g = 0.1$ μm and $\sigma = 2.0$.

In order to estimate the effects of coagulation on the optical properties of smoke, more and better measurements of smoke size distributions and extinction cross sections (e.g. refractive index) are needed. However, based on reasonable estimates of these parameters, coagulation within the plume above the fire does not significantly change the smoke extinction cross section.* The particles do, however, coagulate enough in one hour's time so that any further coagulation, on longer time scales, will act to decrease the cross section. Finally, coagulation on longer time scales, appropriate to global scale climate models, can decrease the extinction coefficient for smoke by 40% or more.

Acknowledgements

This work was performed under the auspices of the U.S Department of Energy by the Lawrence Livermore National Laboratory under Contract W-7405-Eng-48.

* For some fires, dust and large ash particles may be lofted with the smoke plume. In this case, for high enough density, the extinction cross section may decrease significantly due to coagulation of small particles with very large particles (Porch et al., 1985).

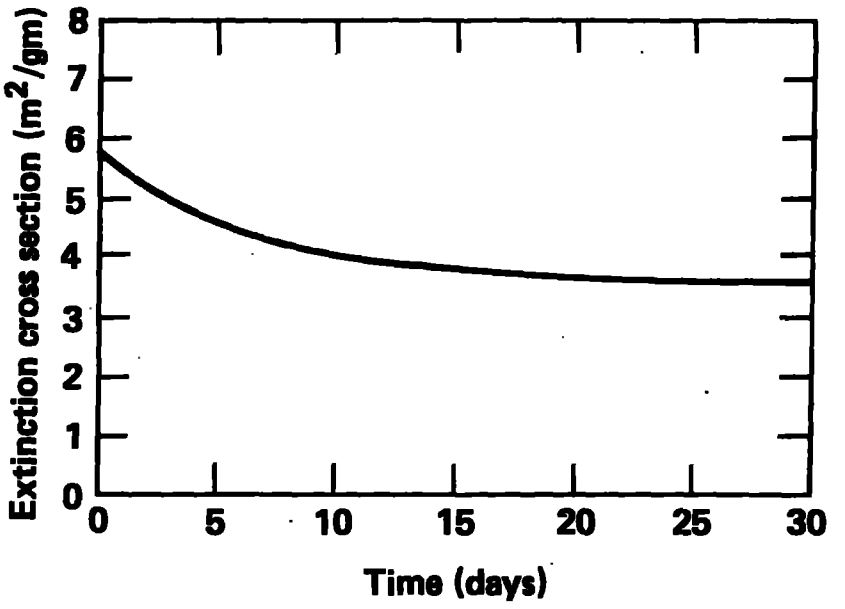

Initial mass loading = 8. X 10^{-10} gm/cm^3

Loading after 30 days = 6.7 X 10^{-11} gm/cm^3

* Extinction coefficient was calculated assuming a refractive index of 1.75−0.3i and initial urban smoke distribution with $r_g = 0.1$, $\sigma_g = 2.0$

Figure 20. Effect of coagulation within the global smoke plume on the extinction cross section. The extinction cross section was calculated assuming a refractive index of 1.75–0.3 i.

REFERENCES

Bard, S. and P. J. Pagni (1981), "Carbon Particulate in Small Pool Fire Flames," *J. of Heat Transfer, 103,* 357–362.

Bankston, C. P., R. A. Cassanova, E. A. Powell, and B. T. Zinn (1978), "Review of Smoke Particulate Properties Data for Burning Natural and Synthetic Materials," *National Bureau of Standards Report* #NBS-GCR-78-147.

Cotton, W. R. (1984), "A Simulation of Cumulonimbus Response to a Large Firestorm - Implication to a Nuclear Winter," *submitted to American Scientist.*

Haselman, L. C. (1980), "TDC - A Computer Code for Calculating Chemically - Reacting Hydrodynamic Flows in Two Dimensions," *Lawrence Livermore National Laboratory Report* UCRL-52931.

MacCracken, M. C. and J. J. Walton (1984), "The Effects of Interactive Transport and Scavenging of Smoke on the Calculated Temperature Change Resulting from Large Amounts of Smoke," *paper presented at the 4th International Conference on Nuclear War,* Erice, Sicily, August 20–24.

Patterson, E. M. and C. K. McMahon (1984), "Absorption Characteristics of Forest Fire Particulate Matter," *Atmospheric Environment, 18,* 2541–2551.

Penner, J. E., L. C. Haselman, Jr. and L. L. Edwards (1985), "Smoke Plume Distribution Above Large Scale Fires: Implications for Simulations of "Nuclear Winter", *submitted to J. Climate and App. Meteor., also Lawrence Livermore National Laboratory Report* UCRL-90915-Rev. 1

Porch, W., J. E. Penner, and D. Gillette (1985), "Parametric Study of Wind Generated Supermicron Particle Effects in Large Fires," *manuscript in preparation.*

Ward, D. E. (1984), *personal communication.*

Turco, R. P., O. B. Toon, T. Ackerman, J. B. Pollack, and C. Sagan (1983), "Nuclear Winter: Global Consequences of Multiple Nuclear Explosions," *Science, 222,* 1283–1292.